frontiers | Frontiers in Built Environment

TYPE Original Research
PUBLISHED 13 October 2022
DOI 10.3389/fbuil.2022.999740

OPEN ACCESS

EDITED BY
Hosam Saleh,
Egyptian Atomic Energy Authority, Egypt

REVIEWED BY
Adewumi John Babafemi,
Stellenbosch University, South Africa
Xiaomei Wan,
Qingdao University of Technology, China
Majid Rostami,
K.N.Toosi University of Technology, Iran

*CORRESPONDENCE
Yaqing Jiang,
yqjiang@hhu.edu.cn
Zhenming Li,
z.li-2@tudelft.nl

SPECIALTY SECTION
This article was submitted to Construction Materials, a section of the journal Frontiers in Built Environment

RECEIVED 21 July 2022
ACCEPTED 30 September 2022
PUBLISHED 13 October 2022

CITATION
Yin K, Jiang Y, Wang Y, Zhao W, Pan Z and Li Z (2022), Effect of rice straw powder on properties of one-part alkali-activated slag.
Front. Built Environ. 8:999740.
doi: 10.3389/fbuil.2022.999740

Effect of rice straw powder on properties of one-part alkali-activated slag

Kangting Yin[1], Yaqing Jiang[1]*, Yu Wang[1], Wenhao Zhao[1], Zhenghua Pan[1] and Zhenming Li[2]*

[1]College of Mechanics and Materials, Hohai University, Nanjing, China, [2]Department of Materials and Environment (Microlab), Faculty of Civil Engineering and Geoscience, Delft University of Technology, Delft, Netherlands

One-part alkali-activated slag (AAS) as a binder material has a promising application in the construction industry. The properties of one-part AAS incorporating agricultural wastes have been seldom studied. In this paper, the fresh and hardened properties of one-part AAS with the addition of rice straw powder (RSP) were investigated. The reaction rate in the acceleration period of AAS is reduced by RSP. The compressive strength of the mixture decreases with the introduction of RSP, while the flexural strength increases. The porosity of the hardened mixtures becomes lower when RSP was incorporated. N-(C)-A-S-H gel was detected in the system when 4.2% RSP was present. The RSP reduces the early-age autogenous shrinkage of AAS by providing internal curing to the matrix, but its effect on long-term drying shrinkage is limited.

KEYWORDS

one-part material, alkali-activated slag, rice straw powder, hydration, microstructure

1 Introduction

The usage of alkali-activated materials (AAMs) as binder materials has been demonstrated to be promising in construction industry. With industrial by-products or waste as precursors, the use of AAMs adds value to the sustainability of the construction sector (Shi et al., 2020; Chindaprasirt et al., 2022; Sadeghian et al., 2022). Alkali-activated binders typically include two-part and one-part or "just add water" binders. The two-part alkali-activated binder is prepared by liquid alkali solution, while the one-part alkali-activated binder involves a dry mix of precursor and solid activators with the addition of water. Without the use of a liquid activator, which is toxic and inconvenient to store and transport, the latter system is easier and safer to prepare by workers (Luukkonen et al., 2018; Sadeghian et al., 2022). Agricultural wastes (e.g., rice straw or husk fibers and ashes) are renewable materials with rich resources, economy, and environmental protection (Ardanuy et al., 2015; Van Nguyen and Mangat, 2020). Many researchers have studied the influences of pre-treated rice straw on OPC and AAMs systems (Xu et al., 2012; Hwang and Huynh, 2015; Xia et al., 2018). It was discovered that incorporating these agricultural wastes improved the mechanical properties and

microstructure of the OPC system. Rice straw fibers, for example, reduce the cost of cement bricks while also providing greater insulation and fire resistance (Xia et al., 2018). Rice husk ash (RHA) has been used as natural pozzolans in OPC concrete systems (Huang et al., 2017). RHA can react with the calcium hydroxide phase produced by cement hydration to form the calcium hydrated silicate and other gelling compounds, resulting in excellent mechanical properties and environmental sustainability (Zareei et al., 2017; Miller et al., 2019). Likewise, studies on the mechanical properties and microstructure of AAMs with agricultural wastes as precursors have also been conducted (Hwang and Huynh, 2015; Sturm et al., 2016). The addition of rice straw fibers, for example, has a considerable impact on improving strength and compensating for dry shrinkage in AAMs (Van Nguyen and Mangat, 2020). However, the properties of one-part alkali-activated slag (AAS) incorporated with agricultural wastes have been seldom studied until now.

One of the main disadvantages of AAMs is their large shrinkage (e.g., autogenous and drying shrinkage), which is relevant for both one-part and conventional AAMs (Ye and Radlińska, 2016; Luukkonen et al., 2018). Some literature documented that the shrinkage of AAS can be up to 6 times that of OPC peers (Ye et al., 2017; Omelchuk et al., 2018). Internal curing agents (Jiang et al., 2021; Yang et al., 2021), shrinkage-reducing admixtures (SRA) (Palacios and Puertas, 2005; Ye et al., 2020), and heat curing (Aydın and Baradan, 2012; Humad et al., 2019) have all been investigated as methods to reduce the high shrinkage of alkali-activated binders. According to previous research (Jiang et al., 2021; Yang et al., 2021), internal curing agents such as superabsorbent polymer and lightweight aggregate can significantly mitigate the autogenous shrinkage of AAS by relieving capillary stresses, but this strategy compromises the early age compressive strength of AAMs and is ineffective in reducing the drying shrinkage of AAMs. When compared to the control sample, the addition of a shrinkage-reducing admixture (SRA) can lower the drying shrinkage of the system by approximately half (Palacios and Puertas, 2005; Ye et al., 2020). Expansive additives used in OPC, such as MgO-type and gypsum, have the potential to reduce the drying shrinkage of AAS. It has been found, for example, that adding higher than 5% highly-reactive MgO reduces the drying shrinkage of AAS at an early age (Jin et al., 2014). Bakharev et al. (2000) discovered that adding 6% gypsum in AAS can significantly lower the drying shrinkage due to the compensating effects of AFt and AFm phases. Heat curing has been employed in some studies to reduce shrinkage (Jiang et al., 2021; Yang et al., 2021). It has been found that the condensation of C-A-S-H during high-temperature curing may result in the formation of a coarse porosity microstructure that reduced effective capillary stress (Bakharev et al., 1999). The shrinkage of one-part AAS is also considerable according to (Coppola et al., 2020; Yin et al., 2022) and seems to be smaller than the two-part AAS (Yin et al., 2022). The difference between shrinkage reduction of one-part AAS and conventional AAS has not yet been reported to our knowledge. In addition, the effective shrinkage compensating techniques of one-part AAS is still lacking. It would be beneficial if the incorporation of agricultural wastes could mitigate the shrinkage of the AAS system.

The goal of the current paper is to explore the feasibility to incorporate an agricultural waste, rice straw powder (RSP), into the one-part AAS system. Firstly, the incorporation of RSP on the setting time and reaction kinetics of AAS paste with and without RSP are investigated. Then, the effect of RSP on the microstructure of AAS pastes is analyzed. X-ray diffraction (XRD), Scanning Electron Microscope (SEM), Energy Dispersive Spectroscopy (EDS) tests and Mercury intrusion porosimetry (MIP) are conducted to characterize the hydration products and the pore structure of the hardened mixtures. ^{1}H nuclear magnetic resonance (NMR) tests are used to evaluatethe possible internal curing effect of RSP. Finally, the autogenous, drying shrinkage, and mechanical properties of the mixtures are studied. The results of this paper are valuable for the application of one-part AAMs with the incorporation of agricultural wastes.

2 Experimental

2.1 Materials and sample preparation

The ground granulated blast furnace slag (hereafter denoted as slag) was used as the main precursor. Solid anhydrous sodium silicate powders and analytic reagent-grade solid flake sodium hydroxide were used as solid activators. The content of the former ingredient was 76.9% SiO_2 and 23.1% Na_2O (i.e. molar ratio: SiO_2/Na_2O = 3.4). The density of the solid anhydrous sodium silicate powder was 2.4 g/cm^3. The alkalis do show a high carbon footprint compared to cement and slag, but due to the relatively low dosage of the alkalis (usually <10%), the overall CO_2 emission and embedded energy per ton of binder are still much lower than OPC systems, according to (Provis and Bernal, 2014). Several studies have been conducted on alternative activators like Na_2CO_3 and Na_2SO_4, but the mechanical properties of the binders are relatively low (Wang et al., 1994; Abdalqader et al., 2016) due to the low pH. For one-part AAS, we expect the strength would be even lower since there is no alkali solution immediately available and the reaction of slag relies on the dissolution of Na_2CO_3 and Na_2SO_4 which provide too low OH^-. Tap water was used for the mixing. The RSP Figure 1A was obtained from ball milling of rice straw fibers, which was provided from a locally harvested field in Anhui province of China. The RSP was collected and passed a No. 60 sieve (the mesh size is 0.3 mm). The density of RSP was 1.4 g/cm^3. The

FIGURE 1
(A) particle morphology and **(B)** SEM morphology of rice straw powder.

TABLE 1 Chemical composition of slag and RSP (wt. %).

Materials	SiO_2	CaO	Al_2O_3	MgO	Fe_2O_3	Na_2O	K_2O	SO_3	P_2O_5	LOI
Slag	30.95	36.59	16.84	9.79	0.36	0.61	0.35	2.55	0.02	0.96
RSP	56.74	12.12	5.5	4.41	0.96	4.7	8.28	2.58	1.87	76.5

contents of cellulose, hemicelluloses, and lignin in the rice straw powders were 28.4%, 27.3%, and 4.4%, respectively, according to the Van Soest method (Van Soest, 1965). Three repetitions of every sample were done. The chemical compositions of slag and RSP are given in Table 1, based on X-ray fluorescence (XRF). It can be seen that the RSP involved fibrous and prismatic-shaped particles, as shown in Figure 1B. The particle size distributions determined by laser diffraction (GSL-101BI, Liaoning) were displayed in Figure 2. To obtain the particle distribution of the testing samples, 2–3 mg of the powder was first poured into a transparent rectangular glass container filled with alcohol, then the glass container was placed in an ultrasonic cleaner (KQ218, Kunshan) for ultrasonic dispersion for 5 min, the glass container was further placed into the groove of a laser particle distribution meter for testing. Finally, the results were measured by the corresponding particle analysis software on the computer connected to the instrument. The mean particle diameters determined by laser diffraction of slag and RSP were 10.6 μm and 165.5 μm, respectively.

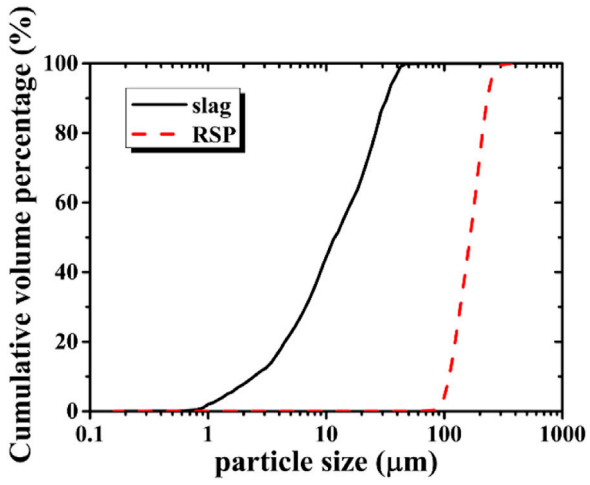

FIGURE 2
The particle size distributions of slag and rice straw powder.

2.2 Mix proportions

The water glass moduli and the Na_2O dosage were fixed at 1.5 and 4% by mass of slag for all the mixtures. The volumetric contents of RSP were the ratio of the volume of the RSP to the volume of precursor (slag). The volumetric contents of RSP were 1.0%, 2.1% and 4.2%, corresponding to 0.5 wt. %, 1 wt. % and 2 wt. %. The mixed proportions of the mixtures were shown in Table 2. The water/solid ratio of the mixtures was 0.41. The mixing process of AAS pastes involved the dry blending of solid materials first for 3 min manually to obtain a homogeneous mixture. Then water was added to the mixture by stirring. The mixtures were continuously stirred at 140 rpm for 2 min, then stopped for 15s, and stirred at 285 rpm for another 2 min.

TABLE 2 Mix proportions of alkali-activated slag pastes.

Mixture	Slag (g)	Na_2O (g)	SiO_2 (g)	Water (g)	RSP (vol. %)
Control	1,000	40	60	450	0
RSP1.0					1.0
RSP2.1					2.1
RSP4.2					4.2

2.3 Experimental part

2.3.1 Setting and hydration heat

The initial and final setting time of the pastes was measured by a Vicat apparatus (Standardization Administration of the People's Republic of China, 2011). An eight-channel isothermal calorimeter with a temperature of 20 ± 0.02°C and a minimum detection limit of 4 μW was used to measure the hydration heat of AAS pastes. To obtain a homogeneous mixture, 10 g of pre-mixed powders and 4.43 g of water were placed into the plastic bottles with an inner diameter of 24.5 mm and manually stirred for 2 min. The bottles were then sealed and transported to the chamber. The entire procedure took around 10 min. The evolution of hydration heat and cumulative heat were tracked for 3 days. The reaction heat results are normalized by the weight of slag.

2.3.2 Microstructure characterization

The pore structure of the samples was measured by a MIP test carried out with MicroActive AutoPore V9600. The samples after 28 days of moist curing (constant temperature of 20°C and relative humidity >99%) were broken into small pieces with a maximum size of 5 mm and then placed in a large volume of isopropanol for 7 days. The isopropanol was replaced by a new one after 1 and 3 days. The samples were then dried in a desiccator under vacuum for 7 days.

The low-field ^{1}H NMR instrument (MacroMR) of Suzhou Niumai Analytical Instrument Corporation was conducted for the ^{1}H NMR test. The constant magnetic field was 0.3 T. The length of the π/2 rf pulse (P1) and π rf (P2) pulse was 7 and 13.04 μs, respectively. The transverse relaxation time (T_2) of free water and RSP-entrained water in the pastes was determined using the Carr-Purcell-Meiboom-Gill (CPMG) methods (Zhou et al., 2018; Jiang et al., 2021). To improve the signal to noise ratio of the CPMG relaxation time measurements, eight repeated scans were performed. The room temperature was kept constant at 20 ± 2°C throughout the testing period. The measurement was conducted on paste cured for 1 day and 7 days with moist curing.

The prepared samples after 28 days of moist curing were ground to pass through a 75-micron sieve prior, then they were placed in anhydrous ethanol to stop hydration for at least 3 days. The samples were further dried for 3 days under vacuum. They were collected for the XRD tests, which were carried out on a Rigaku Smartlab9 X-ray diffractometer, with a tube setting of 40 kV and 150 mA. The step size is 0.02° and the scan rate is 8°/min. The XRD data were collected in the 2θ range of 5–90°.

Some powders were also gold-coated for SEM and EDS tests, which were carried out on a high-resolution Schottky field emission (FEI 400FEG). The SEM test was used to observe the surface of the powder particles. One of the three points in the EDS test was chosen in the region of reaction products for EDS analysis.

TABLE 3 Setting times of AAS mixtures.

Specimen	Control	RSP1.0	RSP2.1	RSP4.2
Initial setting (min)	78	136	230	350
Final setting (min)	158	210	340	450

2.3.3 Compressive strength and flexural strength

40 × 40 × 160 mm^3 alkali-activated slag specimens were prepared according to NEN-196–1 (NEN 196-1, 2005). The compressive strength and flexural strength of the specimens were tested at 1 day, 7 days, and 28 days with moist curing. Compressive strength tests were performed on the broken half prisms from the flexural strength tests.

2.3.4 Autogenous and drying shrinkage

The autogenous shrinkage test was conducted under sealed conditions. The fresh AAS pastes were poured into molds with dimensions of 25 × 25 × 280 mm and sealed by plastic film. The specimens were wrapped in plastic films after 12 h of demolding, set as the zero time. When we measured the lengths of specimens after 24 h demolding, the initial deformation during the 24 h of mixing was ignored. However, the autogenous shrinkage of AAS systems develops quickly in the early stages. Hence, we intended to remove the molds as soon as possible to get early autogenous shrinkage results. Finally, the zero time of 12 h instead of 24 h was chosen due to the difficulty in demolding and consideration of the integrity of the test specimens. The mass loss of the specimens was within 0.1 g during the measurements. The lengths of specimens were measured using a digital comparator. The comparator had a resolution of 0.01 mm.

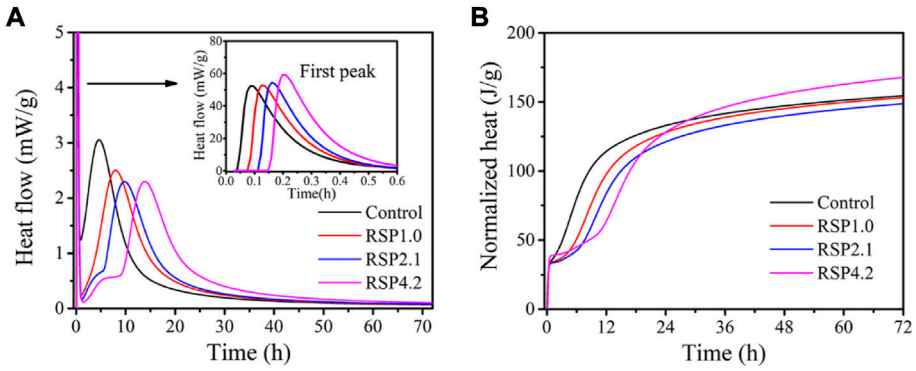

FIGURE 3
(A) Cumulative heat flow and **(B)** cumulative heat of AAS mixtures with and without RSP.

The drying shrinkage measurements were started after demolding at 24 h, which is unlike the foregoing autogenous shrinkage test. They were exposed to a curing chamber with a constant relative humidity of 50% after measuring the initial lengths. The length and mass loss of AAS samples were recorded regularly. These two tests were both conducted at a constant temperature of 20°C.

3 Results and discussion

3.1 Setting times

Table 3 presents the setting time of the AAS mixtures with and without RSP. The control mixture has an initial setting time of 78 min and a final setting time of 158 min. It can be seen that the initial and final setting times of the mixtures are delayed after adding RSP. The RSP4.2 has initial and final setting times of 350 min and 450 min, respectively. This is related to the cellulose in RSP undergoing chemical reactions in an alkaline environment. This leads to various acids being generated and neutralized with hydroxide ions to produce salts. These salts accumulate on hydration products and prolong the setting time of AAS, as described in (Yun Yang and Montgomery, 1996; Guo and Wu, 2008; Doudart de la Grée et al., 2017; Choi and Choi, 2021). The retarding properties produced by RSPs can improve the open time of alkali-activated slag during construction.

3.2 Reaction kinetics

The heat evolution curves of the AAS pastes with and without RSP are shown in Figure 2. It was found that the mixtures all show two peaks in the heat flow curves (Figure 3A). The first peak is dominated by the dissolution of slag grains and solid activators, whereas the second peak is attributed to the formation of the major aluminosilicate gels (Tu et al., 2019). In addition, it also can be seen that the first peak of RSP-based pastes exhibits a moderate delay compared to the control sample. This can be attributed to the fact that RSP has larger particle sizes than slag, which results in less slag-activation solution contact and a delayed dissolution of the slag. After the induction period, the addition of RSP reduces the intensity of the main peak. As indicated in Section 3.1, RSP can be degraded in an alkaline environment to produce acids such as glycolic acid and lactic acid and then neutralized with OH^- (Yun Yang and Montgomery, 1996; Guo and Wu, 2008; Doudart de la Grée et al., 2017). This may be contributed to a lower pH of the RSP-based AAS system. Hence, the heat flow of the AAS pastes decreases upon the addition of RSP.

The accumulated heat results likewise exhibit the aforementioned impacts. Figure 3B demonstrates that the

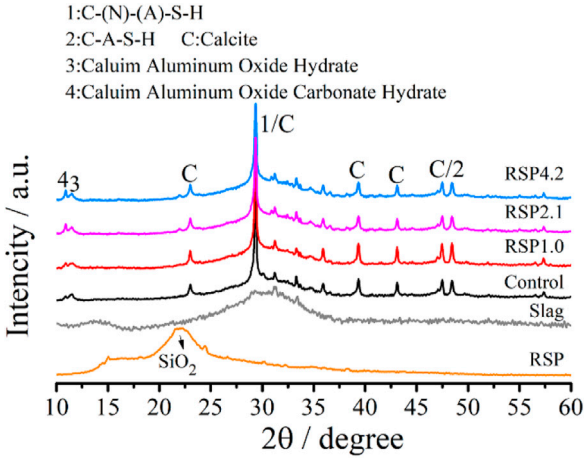

FIGURE 4
XRD patterns of the AAS mixtures with and without RSP after 28 days of curing.

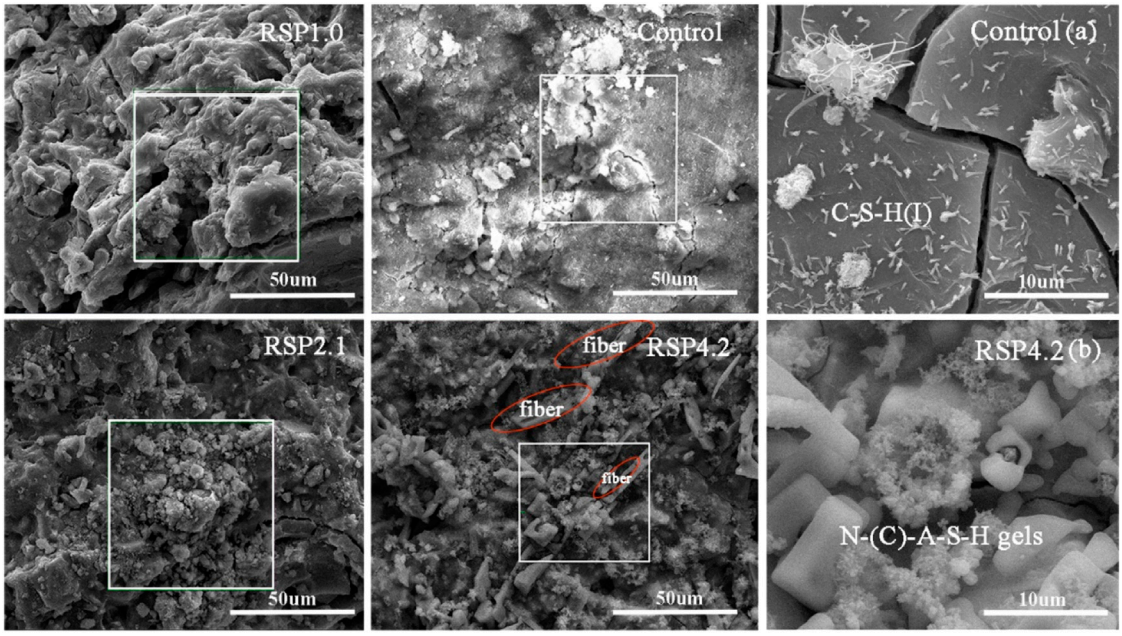

FIGURE 5
Morphologies of **(A)** control and **(B)** RSP4.2 paste and EDS analysis of the AAS paste with and without RSP at 28 days.

cumulative heat of RSP1.0 and RSP2.1 pastes are lower than that of the control sample after the deceleration period. However, the cumulative heat of RSP4.2 pastes becomes higher in the long run. This suggests that the addition of 4.2% RSP enhances the reaction of the AAS in the long run and increases the amount of hydration products, as will be mentioned in the next section. It also can be noticed that the final cumulative hydration heat of the four AAS pastes increased to 150J/g until 72 h, which was about half that of the common heat release of OPC pastes with the same w/b of 0.45 (Brough and Atkinson, 2002). This finding is consistent with the results of one-part and conventional AAS mixtures (Li et al., 2019a; Kim et al., 2019).

3.3 Hydration products

Figure 4 presents the XRD patterns of the AAS mixtures with and without RSP at the age of 28 days. It can be found that slag was mostly amorphous (Ye and Radlińska, 2016). The SiO_2 can be seen in the XRD pattern of RSP. From the X-ray diffractograms for AAS paste, the peaks at 29° and 49.8° represent the formation of C-(N)-(A)-S-H (denoted as "1") and C-A-S-H (denoted as "2") gels (Ben Haha et al., 2011; Kovtun et al., 2015). They were the main hydration products of the AAS system, as described in (Li et al., 2019a; Qu et al., 2020). Calcium aluminum oxide hydrate and calcium aluminum oxide carbonate hydrate are also found in RSP-based pastes, especially for the RSP2.1 and RSP4.2 pastes. All pastes contain calcite ($CaCO_3$), which can be related to atmospheric carbonation (Jiao et al., 2018). Similar results also can be obtained in (Ben Haha et al., 2011; Kovtun et al., 2015). Compared to the results as reported in (Yin et al., 2022), rice straw ash from burning of rice straw and rice straw powders from shredding have different influences on AAS due to their different physical and chemical properties. The rice straw ash results in the anisotropic growth of the formed crystals, which can partially compensate for the autogenous shrinkage of the pastes. While it seems that RSP used in this study leads to no distinct changes in the main hydration products of the AAS binder according to the XRD data. In addition, distinct differences in the morphologies of the C-S-H can be observed between RSP4.2 and control pastes, as will be analyzed below.

Figure 5 shows the microstructure of the control and RSP-based pastes at 28 days Figure 5A and Figure 5B display the SEM image of control and RSP4.2 pastes. Some cracks can be observed in Figure 5A. This can be attributed to the shrinkage during curing or sample preparation (Li et al., 2021). Small amounts of C-S-H (I) can also be found attached to the matrix phases, which is consistent with the results of (Ren et al., 2021). Figure 5B reveals that a substantial amount of N-(C)-A-S-H gel (petal-shaped) accumulated into clusters in the RSP4.2 sample, as indicated in the reaction kinetics analysis. The RSP4.2 sample also has flake fibers, as marked

TABLE 4 EDS determination of atomic ratio.

Code Spectrum number	Si/Al	Ca/Si	Na/Al	Mg/Al
Control	1.81	1.31	0.62	0.64
RSP1.0	3.26	0.87	1.29	0.64
RSP2.1	2.70	0.98	0.84	0.69
RSP4.2	3.74	0.73	7.67	0.57

by red circles. As the fibers become intertwined, the compressive strength decreases due to the agglomeration of the fibers. Similar results can be found as described in (Alomayri, 2017).

Table 4 displays the EDS results of the selected zone of the hardened mixtures at 28 days. In comparison to the control sample, the Ca/Si ratios of the RSP1.0, RSP2.1, and RSP4.2 samples are lower. The lower Ca/Si ratios of AAS pastes appear to have a denser microstructure, especially for the RSP4.2 sample (Figure 5B). The Si/Al ratio of the control sample was 1.81, which is supported by the results reported by Jiao et al. (Lloyd et al., 2010; Jiao et al., 2018). The RSP1.0, RSP2.1, and RSP4.2 samples have Si/Al ratios of 3.26, 2.70, and 3.74, respectively, indicating that Si-O bonds were generated more in AAS specimens. As shown in Table 4, the Na/Al ratio of RSP-based pastes increases, implying that Na^+ eventually integrates into the gel products. It can be seen that N-A-S-H gel was generated in RSP4.2 (Figure 5B), and the other mixtures were not detected. This may be the reason for the significantly high Na/Al for RSP4.2 compared to other mixtures. This is related to cellulose in RSP is more likely to dissolve and precipitate in an alkaline environment. Hence, the sodium contained in RSP can be released to participate in the formation of N-(C)-A-S-H gels (Doudart de la Grée et al., 2017). Further studies are still necessary to reveal the mechanism of this phenomenon.

3.4 Pore-related properties

Figure 6 shows the pore size distribution and cumulative intrusion of the AAS mixtures at 28 days. According to (Jiao et al., 2018), Table 5 depicts the classification of pores. Table 6 lists the results of the volume proportion, average pore sizes, and porosity of the hardened mixtures. The porosity discussed here is the total porosity of pastes. From Table 6, It can be found that the volume proportion of mesopores of RSP-based AAS mixtures was all increased. The volume proportion of mesopores of RSP4.2 paste is 8.6% higher than that of the control samples. It can be noted that RSP-based AAS pastes had a lower volume proportion of voids and microcracks. In addition, the porosity of AAS hardened pastes decreases upon the introduction of RSP. The porosity of RSP1.0, RSP2.1, and RSP4.2 paste is 9.2%, 8.2%, and 5.8% lower than that of the control pastes. These may be explained by that the adsorption of the mixing water by the presence of RSP (Vargas et al., 2017). By decreasing the mixing water, less porosity is generated. Furthermore, the formation of hydration products (Figure 4) is also responsible for the decreased porosity of AAS binders.

3.5 Relaxation distribution and liquid status

The ^{1}H NMR method reveals the internal curing effect of RSP in AAS during the hydration process. The transverse relaxation time (T_2) of control and RSP4.2 paste is shown in Figure 7. It can be seen that the T_2 distributions of the two mixtures mainly fall in 0.1–100 ms, which corresponds to the signal of capillary water (Liu et al., 2021). The initial single peak at T_2 of 0.1–10 ms shifts left from 1 day to 7 days, which indicates that the pore structure is dense due to the continuous production of hydration products (Jiang et al.,

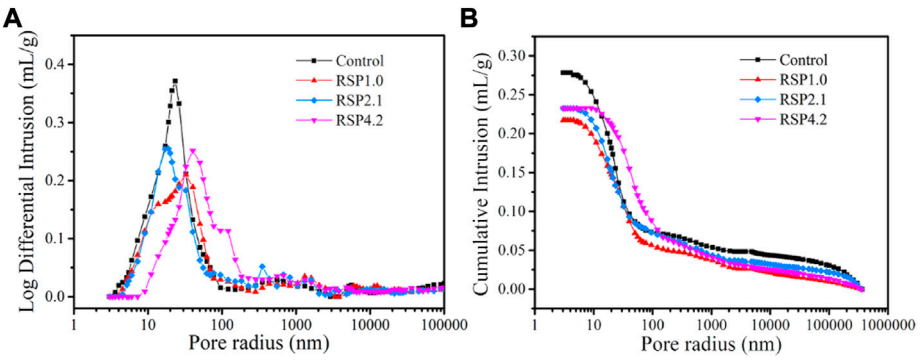

FIGURE 6
(A) Differential intrusion and **(B)** cumulative intrusion of AAS mixtures with and without RSP at 28 days.

TABLE 5 Classifications of pores in the AAS pastes.

	Micropores	Mesopores	Macropores	Voids and microcracks
Pore size/nm	<2.5	2.5–50	50–10000	>10,000

According to the International Union of Pure and Applied Chemistry system.

TABLE 6 Volume proportion, average pore sizes, and porosity of hardened mixtures at 28 days.

Specimen	Volume proportions (%)			Average pore size (4V/A) (nm)	Porosity (%)
	Mesopores	Macropores	Voids and microcracks		
Control	61.68	26.27	12.05	22.07	35.46
RSP1.0	68.77	24.64	6.58	23.58	32.20
RSP2.1	62.49	27.17	10.34	24.56	32.57
RSP4.2	67.00	26.27	6.73	47.98	33.41

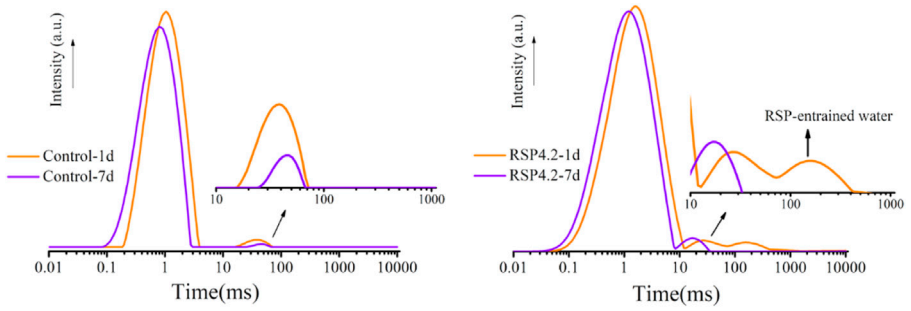

FIGURE 7
T_2 distributions of AAS mixtures with and without RSP for selected hydration times.

2021; Liu et al., 2021). With increasing hydration time, the intensity of the T_2 peak dropped, implying that free water was continuously consumed and transformed into chemical-bound water.

In the RSP4.2 mixtures at 1 day, an extra signal arises in the range of 100–1,000 ms. This is due to the entrained water in RSP, which is comparable to the signal observed in binders containing superabsorbent polymers (SAP) (Jiang et al., 2021; Zhong et al., 2021). This peak suggests that RSP can act as an internal curing agent in one-part AAS. The hump representing RSP-entrained water is not visible at the age of 7 days, which suggests that the water was gradually consumed as evidence of internal curing. This is also analogous to the internal curing of porous ashes such as RHA, which has been used for a long in cementitious systems (Van et al., 2014; Kang et al., 2019).

3.6 Mechanical properties

The compressive strength of the mixtures incorporating 1.0%, 2.1%, and 4.2% RSP is shown in Figure 8. As can be seen in Figure 8A, the compressive strength of the AAS mixtures increases over time. Compared with the control pastes, the compressive strength of RSP1.0, RSP2.1, and RSP4.2 samples show a lower magnitude of the reduction of the compressive strength with time. This is because RSP, which serves as internal curing by absorbing moisture during mixing (Section 3.5). At 28 days, the early-age strength shows a significant reduction as 4.2% RSP was added to the specimens. In addition to the internal curing by SAP between specimens, the decreased hydration rates at early ages of RSP-modified AAS binders are also a reason for this result (Figure 3). Furthermore, the decreased compressive strength with 4.2% RSP also may be related to the higher volume

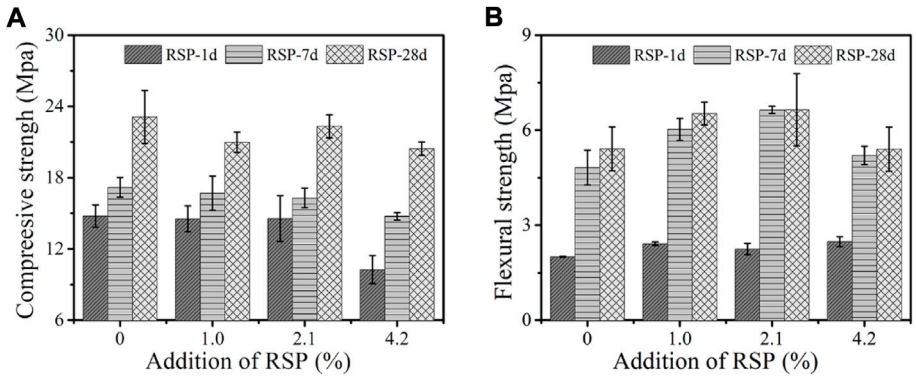

FIGURE 8
Effect of RSP content on **(A)** compressive strength and **(B)** flexural strength of AAS mixtures after 1 day, 7 days and 28 days of curing.

proportion of mesopores in the matrix, as indicated in Section 3.4.

As shown in Figure 8B, the incorporation of RSP increases the flexural strength of AAS mixtures. For example, compared with the control samples, the flexural strength of RSP1.0, RSP2.1, and RSP4.2 specimens at 1 day increased by 20.5%, 12.3%, and 24.0%, respectively. Similar trends can be seen in the flexural strength of the mixtures at 7 days and 28 days. The improved flexural strength indicates a strong bonding between RSP particles and the AAS matrix. Compared to other fibers like PVA fibers, the surface of the fibrous RSP is rougher (see Figure 1B) (Vargas et al., 2017). The RSP particles can be more closely embedded in the matrix by their bridge effect, thus the flexural strength of the mixtures is improved (Alomayri et al., 2013). Similar observations also can be seen in (Venkatesan and Pazhani, 2016). Also, the dense and thinner ITZ coupled with the porous RSP can be another reason for the enhancement in the flexural strength, similar to the Lightweight aggregates (LWA) concrete as described by Vargas et al. (2017). As indicated in Table 6, the lower volume proportion of voids and microcracks also relates to the higher flexural strength.

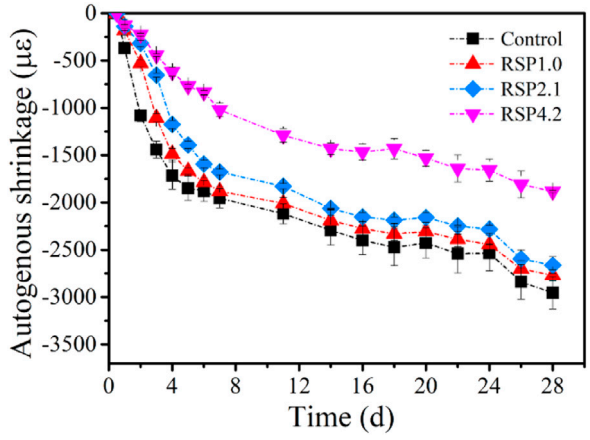

FIGURE 9
Autogenous shrinkage of AAS mixtures with and without RSP.

3.7 Autogenous shrinkage

Figure 9 demonstrates that the control mixture has an autogenous shrinkage of around 2000 μm/m at 7 days. The autogenous shrinkage at 28 days is 3000 μm/m. According to (Li et al., 2019a; Kim et al., 2019; Tu et al., 2019; Li et al., 2020a; Qu et al., 2020), the autogenous shrinkage of AAMs ranges from 2000 to 10,000 μm/m within 28 days. It seems that the autogenous shrinkage of the one-part AAS in this paper was smaller than the conventional AAS. It is worth noting that the autogenous shrinkage within the first 12 h was not measured in this paper. Nonetheless, the autogenous shrinkage of one-part AAS pastes in this paper was roughly 4 times larger than that of the OPC paste (w/c = 0.4) (Li et al., 2020a).

The autogenous shrinkage of AAS pastes becomes lower when RSP is present, especially at a very early age, as shown in Figure 9. This is also related to the decreased reaction rate due to the internal chemical reaction of the AAS pastes with the addition of RSP (see Figure 3). After 7 days, the reduction of the autogenous shrinkage for RSP1.0 and RSP2.1 paste is not obvious, which may be related to the low content of RSP. However, the RSP4.2 paste shows an autogenous shrinkage reduction of 47.8% at 7 days, as compared to the control paste. This mitigating effect is already comparable to the effect of SAP (Tu et al., 2019; Li et al., 2020b). These results suggest that RSP can be employed as an effective shrinkage-mitigating admixture for one-part AAS considering also comparable

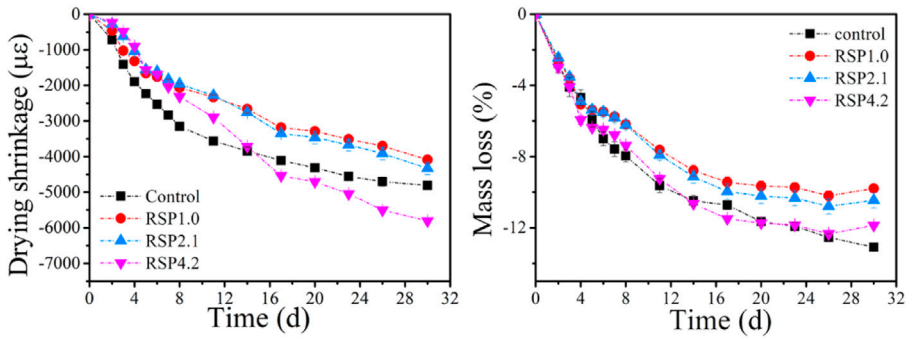

FIGURE 10
Drying shrinkage and mass loss of AAS paste with and without RSP.

strength. As indicated in Section 3.5, the reason for the decreased autogenous shrinkage is probably due to the internal curing effect of RSP, since the internal curing water begins to be released from the swollen RSP at hardened stage. The moisture loss can be supplemented and thus the deformation caused by self-desiccation and volume reduction of chemical reactants can be restrained by RSP. Similar phenomena have been seen in SAP, LWA, and RHA containing AAS pastes (Kang et al., 2019; Balapour et al., 2020; Jiang et al., 2021). The pore structure of the hardened AAS pastes reveals that the addition of RSP increases the average pore size (see Table 6). This indicates a smaller hygro-mechanical deformation, in line with the above discussion. As a result, specimens with RSP should show a lower autogenous shrinkage.

3.8 Drying shrinkage and mass loss

Figure 10 depicts the development of drying shrinkage and mass loss of AAS samples with and without RSP. It can be seen from Figure 10A that the dry shrinkage of the one-part AAS pastes was only 60% of the drying shrinkage of conventional AAS pastes measured by Qu et al. (2020). According to other literature (Ye et al., 2017; Jiao et al., 2018; Li et al., 2019b; Kim et al., 2019; Qu et al., 2020), one-part AAS paste appears to have a lower drying shrinkage than two-part AAS, implying a positive message for the application of one-part AAS.

The addition of RSP decreases the drying shrinkage of the mixtures at an early age. As shown in Figure 10A, the drying shrinkage is decreased by 32.2%, 35.1%, and 28.1% at 7 days compared to the control sample, respectively. Part of the reason lies in the reduction of the autogenous shrinkage of AAS pastes when RSP is present since the drying or in fact total shrinkage measured in this study was considered a combination of drying and self-induced shrinkages. The addition of RSP can be used as a filler to play a role similar to coarse aggregate in AAS (Gao et al., 2021). However, mixing 4.2% RSP increases the drying shrinkage after 13 days of AAS. The drying shrinkage of RSP4.2 paste is increased by 20.7% at 30 days, as compared to the control paste. It also seems that the drying shrinkage in RSP1.0 and RSP2.1 pastes can exceed that of the control sample after 30 days. The increased drying shrinkage may be related to the results of the internal curing, which can decrease the autogenous shrinkage but is not effective in reducing the drying shrinkage, since the entrapped free water would evaporate at a later age (Gao et al., 2020). In addition, the elastic modulus can also be reduced when RSP is present (as indicated in Figure 8A), which may contribute to larger drying shrinkage. The higher volume proportion of mesopores in RSP mixtures as mentioned in Section 3.4 also can be related to the high drying shrinkage at a later age, as described in (Collins and Sanjayan, 2000; Jiao et al., 2018). The tendency of the mass loss curve is similar to that of the dry shrinkage curve, which shows that the addition of RSP can not hinder the moisture loss of the mixtures.

4 Concluding remarks

In this study, the fresh and hardened properties of one-part alkali-activated slag paste with and without RSP are investigated. The following conclusions can be made:

1. The addition of RSP prolongs the initial and final setting times of the AAS mixtures. The addition of RSP reduces the reaction rate in the acceleration period of one-part AAS.

2. The main products of one-part AAS with and without RSP are C-A-S-H gels. The porosity of AAS mixtures decreases and N-(C)-A-S-H gels are detected upon the addition of 4.2% RSP.

3. The introduction of RSP shows a smaller reduction in

compressive strength of AAS mixtures when compared to the control sample. While the addition of RSP increases the flexural strength of AAS.

4. The introduction of RSP reduces the autogenous shrinkage of AAS pastes, attributed to the internal curing effect of RSP, but its mitigation of drying shrinkage is limited.

Data availability statement

The original contributions presented in the study are included in the article/supplementary materials, further inquiries can be directed to the corresponding authors.

Author contributions

KY: Conceptualization, Investigation, Methodology, Writing—original draft. YJ: Funding acquisition, Resources. YW: Conceptualization. WZ: Investigation. ZP: Investigation. ZL: Methodology, Supervision, Writing—review and; editing.

Funding

This work was supported by the National Natural Science Foundation of China [grant numbers 51738003, 11772120].

Conflict of interest

The authors declare that the research was conducted in the absence of any commercial or financial relationships that could be construed as a potential conflict of interest.

Publisher's note

All claims expressed in this article are solely those of the authors and do not necessarily represent those of their affiliated organizations, or those of the publisher, the editors and the reviewers. Any product that may be evaluated in this article, or claim that may be made by its manufacturer, is not guaranteed or endorsed by the publisher.

References

Abdalqader, A. F., Jin, F., and Al-Tabbaa, A. (2016). Development of greener alkali-activated cement: Utilisation of sodium carbonate for activating slag and fly ash mixtures. *J. Clean. Prod.* 113, 66–75. doi:10.1016/j.jclepro.2015.12.010

Alomayri, T., Shaikh, F. U. A., and Low, I. M. (2013). Characterisation of cotton fibre-reinforced geopolymer composites. *Compos. Part B Eng.* 50, 1–6. doi:10.1016/j.compositesb.2013.01.013

Alomayri, T. (2017). Effect of glass microfibre addition on the mechanical performances of fly ash-based geopolymer composites. *J. Asian Ceram. Soc.* 5, 334–340. doi:10.1016/j.jascer.2017.06.007

Ardanuy, M., Claramunt, J., and Toledo Filho, R. D. (2015). Cellulosic fiber reinforced cement-based composites: A review of recent research. *Constr. Build. Mater.* 79, 115–128. doi:10.1016/j.conbuildmat.2015.01.035

Aydın, S., and Baradan, B. (2012). Mechanical and microstructural properties of heat cured alkali-activated slag mortars. *Mater. Des.* 35, 374–383. doi:10.1016/j.matdes.2011.10.005

Bakharev, T., Sanjayan, J. G., and Cheng, Y. B. (1999). Effect of elevated temperature curing on properties of alkali-activated slag concrete. *Cem. Concr. Res.* 29, 1619–1625. doi:10.1016/S0008-8846(99)00143-X

Bakharev, T., Sanjayan, J. G., and Cheng, Y. B. (2000). Effect of admixtures on properties of alkali-activated slag concrete. *Cem. Concr. Res.* 30, 1367–1374. doi:10.1016/S0008-8846(00)00349-5

Balapour, M., Zhao, W., Garboczi, E. J., Oo, N. Y., Spatari, S., Hsuan, Y. G., et al. (2020). Potential use of lightweight aggregate (LWA) produced from bottom coal ash for internal curing of concrete systems. *Cem. Concr. Compos.* 105, 103428. doi:10.1016/j.cemconcomp.2019.103428

Ben Haha, M., Le Saout, G., Winnefeld, F., and Lothenbach, B. (2011). Influence of activator type on hydration kinetics, hydrate assemblage and microstructural development of alkali activated blast-furnace slags. *Cem. Concr. Res.* 41, 301–310. doi:10.1016/j.cemconres.2010.11.016

Brough, A. R., and Atkinson, A. (2002). Sodium silicate-based, alkali-activated slag mortars - Part I. Strength, hydration and microstructure. *Cem. Concr. Res.* 32, 865–879. doi:10.1016/S0008-8846(02)00717-2

Chindaprasirt, P., Sriopas, B., Phosri, P., Yoddumrong, P., Anantakarn, K., and Kroehong, W. (2022). Hybrid high calcium fly ash alkali-activated repair material for concrete exposed to sulfate environment. *J. Build. Eng.* 45, 103590. doi:10.1016/j.jobe.2021.103590

Choi, H., and Choi, Y. C. (2021). Setting characteristics of natural cellulose fiber reinforced cement composite. *Constr. Build. Mater.* 271, 121910. doi:10.1016/j.conbuildmat.2020.121910

Collins, F., and Sanjayan, J. G. (2000). Effect of pore size distribution on drying shrinking of alkali-activated slag concrete. *Cem. Concr. Res.* 30, 1401–1406. doi:10.1016/S0008-8846(00)00327-6

Coppola, L., Coffetti, D., Crotti, E., Candamano, S., Crea, F., Gazzaniga, G., et al. (2020). The combined use of admixtures for shrinkage reduction in one-part alkali activated slag-based mortars and pastes. *Constr. Build. Mater.* 248, 118682. doi:10.1016/j.conbuildmat.2020.118682

Doudart de la Grée, G. C. H., Yu, Q. L., and Brouwers, H. J. H. (2017). Assessing the effect of CaSO4 content on the hydration kinetics, microstructure and mechanical properties of cements containing sugars. *Constr. Build. Mater.* 143, 48–60. doi:10.1016/j.conbuildmat.2017.03.067

Gao, P., Chen, Y., Huang, H., Qian, Z., Schlangen, E., Wei, J., et al. (2020). Investigation of drying-induced non-uniform deformation, stress, and micro-crack propagation in concrete. *Cem. Concr. Compos.* 114, 103786. doi:10.1016/j.cemconcomp.2020.103786

Gao, P., Chen, Y., Huang, H., Qian, Z., Schlangen, E., Wei, J., et al. (2021). Effect of coarse aggregate size on non-uniform stress/strain and drying-induced microcracking in concrete. *Compos. Part B Eng.* 216, 108880. doi:10.1016/j.compositesb.2021.108880

Guo, Y., and Wu, P. (2008). Investigation of the hydrogen-bond structure of cellulose diacetate by two-dimensional infrared correlation spectroscopy. *Carbohydr. Polym.* 74, 509–513. doi:10.1016/j.carbpol.2008.04.005

Huang, H., Gao, X., Wang, H., and Ye, H. (2017). Influence of rice husk ash on strength and permeability of ultra-high performance concrete. *Constr. Build. Mater.* 149, 621–628. doi:10.1016/j.conbuildmat.2017.05.155

Humad, A. M., Provis, J. L., and Cwirzen, A. (2019). Effects of curing conditions on shrinkage of alkali-activated high-MgO Swedish slag concrete. *Front. Mater.* 6. doi:10.3389/fmats.2019.00287

Hwang, C. L., and Huynh, T. P. (2015). Effect of alkali-activator and rice husk ash content on strength development of fly ash and residual rice husk ash-based geopolymers. *Constr. Build. Mater.* 101, 1–9. doi:10.1016/j.conbuildmat.2015.10.025

Jiang, D., Li, X., Lv, Y., Li, C., Jiang, W., Liu, Z., et al. (2021). Autogenous shrinkage and hydration property of alkali activated slag pastes containing

superabsorbent polymer. *Cem. Concr. Res.* 149, 106581. doi:10.1016/j.cemconres.2021.106581

Jiao, Z., Wang, Y., Zheng, W., and Huang, W. (2018). Effect of dosage of sodium carbonate on the strength and drying shrinkage of sodium hydroxide based alkali-activated slag paste. *Constr. Build. Mater.* 179, 11–24. doi:10.1016/j.conbuildmat.2018.05.194

Jin, F., Gu, K., and Al-Tabbaa, A. (2014). Strength and drying shrinkage of reactive MgO modified alkali-activated slag paste. *Constr. Build. Mater.* 51, 395–404. doi:10.1016/j.conbuildmat.2013.10.081

Kang, S. H., Hong, S. G., and Moon, J. (2019). The use of rice husk ash as reactive filler in ultra-high performance concrete. *Cem. Concr. Res.* 115, 389–400. doi:10.1016/j.cemconres.2018.09.004

Kim, H. J., Tafesse, M., Lee, H. K., and Kim, H. K. (2019). Incorporation of CFBC ash in sodium silicate-activated slag system: Modification of microstructures and its effect on shrinkage. *Cem. Concr. Res.* 123, 105771. doi:10.1016/j.cemconres.2019.05.016

Kovtun, M., Kearsley, E. P., and Shekhovtsova, J. (2015). Chemical acceleration of a neutral granulated blast-furnace slag activated by sodium carbonate. *Cem. Concr. Res.* 72, 1–9. doi:10.1016/j.cemconres.2015.02.014

Li, Z., Nedeljković, M., Chen, B., and Ye, G. (2019a). Mitigating the autogenous shrinkage of alkali-activated slag by metakaolin. *Cem. Concr. Res.* 122, 30–41. doi:10.1016/j.cemconres.2019.04.016

Li, Z., Liu, J., and Ye, G. (2019b). Drying shrinkage of alkali-activated slag and fly ash concrete; A comparative study with ordinary Portland cement concrete. *Heron* 64, 149–163.

Li, Z., Lu, T., Liang, X., Dong, H., and Ye, G. (2020a). Mechanisms of autogenous shrinkage of alkali-activated slag and fly ash pastes. *Cem. Concr. Res.* 135, 106107. doi:10.1016/j.cemconres.2020.106107

Li, Z., Wyrzykowski, M., Dong, H., Granja, J., Azenha, M., Lura, P., et al. (2020b). Internal curing by superabsorbent polymers in alkali-activated slag. *Cem. Concr. Res.* 135, 106123. doi:10.1016/j.cemconres.2020.106123

Li, Z., Lu, T., Chen, Y., Wu, B., and Ye, G. (2021). Prediction of the autogenous shrinkage and microcracking of alkali-activated slag and fly ash concrete. *Cem. Concr. Compos.* 117, 103913. doi:10.1016/j.cemconcomp.2020.103913

Liu, H., Sun, Z., Yang, J., and Ji, Y. (2021). A novel method for semi-quantitative analysis of hydration degree of cement by 1H low-field NMR. *Cem. Concr. Res.* 141, 106329. doi:10.1016/j.cemconres.2020.106329

Lloyd, R. R., Provis, J. L., and Van Deventer, J. S. J. (2010). Pore solution composition and alkali diffusion in inorganic polymer cement. *Cem. Concr. Res.* 40, 1386–1392. doi:10.1016/j.cemconres.2010.04.008

Luukkonen, T., Abdollahnejad, Z., Yliniemi, J., Kinnunen, P., and Illikainen, M. (2018). One-part alkali-activated materials: A review. *Cem. Concr. Res.* 103, 21–34. doi:10.1016/j.cemconres.2017.10.001

Miller, S. A., Cunningham, P. R., and Harvey, J. T. (2019). Rice-based ash in concrete: A review of past work and potential environmental sustainability. *Resour. Conserv. Recycl.* 146, 416–430. doi:10.1016/j.resconrec.2019.03.041

NEN 196-1 (2005). Methods of testing cement–Part 1: Determination of strength. *Eur. Comm. Stand.*

Omelchuk, V., Ye, G., Runova, R., and Rudenko, I. (2018). Shrinkage behavior of alkali-activated slag cement pastes. *Key Eng. Mater.* 761, 45–48. doi:10.4028/www.scientific.net/kem.761.45

Palacios, M., and Puertas, F. (2005). Effect of superplasticizer and shrinkage-reducing admixtures on alkali-activated slag pastes and mortars. *Cem. Concr. Res.* 35, 1358–1367. doi:10.1016/j.cemconres.2004.10.014

Provis, J. L., and Bernal, S. A. (2014). Geopolymers and related alkali-activated materials. *Annu. Rev. Mater. Res.* 44, 299–327. doi:10.1146/annurev-matsci-070813-113515

Qu, Z. Y., Yu, Q., Ji, Y. D., Gauvin, F., and Voets, I. K. (2020). Mitigating shrinkage of alkali activated slag with biofilm. *Cem. Concr. Res.* 138, 106234. doi:10.1016/j.cemconres.2020.106234

Ren, J., Sun, H., Li, Q., Li, Z., Ling, L., Zhang, X., et al. (2021). Experimental comparisons between one-part and normal (two-part) alkali-activated slag binders. *Constr. Build. Mater.* 309, 125177. doi:10.1016/j.conbuildmat.2021.125177

Sadeghian, G., Behfarnia, K., and Teymouri, M. (2022). Drying shrinkage of one-part alkali-activated slag concrete. *J. Build. Eng.* 51, 104263. doi:10.1016/j.jobe.2022.104263

Shi, D., Ye, J., and Zhang, W. (2020). Effects of activator content on properties , mineralogy , hydration and microstructure of alkali-activated materials synthesized from calcium silicate slag and ground granulated blast furnace slag. *J. Build. Eng.* 32, 101791. doi:10.1016/j.jobe.2020.101791

Standardization Administration of the People's Republic of China (2011). *GB/T 1346-2011: Test methods for water requirement of normal consistency, setting time and soundness of the portland cement*. Beijing: China Standards Press, 6. (in Chinese).

Sturm, P., Gluth, G. J. G., Brouwers, H. J. H., and Kühne, H. C. (2016). Synthesizing one-part geopolymers from rice husk ash. *Constr. Build. Mater.* 124, 961–966. doi:10.1016/j.conbuildmat.2016.08.017

Tu, W., Zhu, Y., Fang, G., Wang, X., and Zhang, M. (2019). Internal curing of alkali-activated fly ash-slag pastes using superabsorbent polymer. *Cem. Concr. Res.* 116, 179–190. doi:10.1016/j.cemconres.2018.11.018

Van, V. T. A., Rößler, C., Bui, D. D., and Ludwig, H. M. (2014). Rice husk ash as both pozzolanic admixture and internal curing agent in ultra-high performance concrete. *Cem. Concr. Compos.* 53, 270–278. doi:10.1016/j.cemconcomp.2014.07.015

Van Nguyen, C., and Mangat, P. S. (2020). Properties of rice straw reinforced alkali activated cementitious composites. *Constr. Build. Mater.* 261, 120536. doi:10.1016/j.conbuildmat.2020.120536

Van Soest, P. J. (1965). Use of detergents in analysis of fibrous feeds. III. Study of effects of heating and drying on yield of fiber and lignin in forages. *J. AOAC Int.* 48, 785–790. doi:10.1093/jaoac/48.4.785

Vargas, P., Restrepo-Baena, O., and Tobón, J. I. (2017). Microstructural analysis of interfacial transition zone (ITZ) and its impact on the compressive strength of lightweight concretes. *Constr. Build. Mater.* 137, 381–389. doi:10.1016/j.conbuildmat.2017.01.101

Venkatesan, R. P., and Pazhani, K. C. (2016). Strength and durability properties of geopolymer concrete made with ground granulated blast furnace slag and black rice husk ash. *KSCE J. Civ. Eng.* 20, 2384–2391. doi:10.1007/s12205-015-0564-0

Wang, S. D., Scrivener, K. L., and Pratt, P. L. (1994). Factors affecting the strength of alkali-activated slag. *Cem. Concr. Res.* 24, 1033–1043. doi:10.1016/0008-8846(94)90026-4

Xia, T., Huang, H., Wu, G., Sun, E., Jin, X., and Tang, W. (2018). The characteristic changes of rice straw fibers in anaerobic digestion and its effect on rice straw-reinforced composites. *Ind. Crops Prod.* 121, 73–79. doi:10.1016/j.indcrop.2018.04.004

Xu, W., Lo, T. Y., and Memon, S. A. (2012). Microstructure and reactivity of rich husk ash. *Constr. Build. Mater.* 29, 541–547. doi:10.1016/j.conbuildmat.2011.11.005

Yang, J., Snoeck, D., De Belie, N., and Sun, Z. (2021). Comparison of liquid absorption-release of superabsorbent polymers in alkali-activated slag and Portland cement systems : An NMR study combined with additional methods. *Cem. Concr. Res.* 142, 106369. doi:10.1016/j.cemconres.2021.106369

Ye, H., and Radlińska, A. (2016). Shrinkage mechanisms of alkali-activated slag. *Cem. Concr. Res.* 88, 126–135. doi:10.1016/j.cemconres.2016.07.001

Ye, H., Cartwright, C., Rajabipour, F., and Radlińska, A. (2017). Understanding the drying shrinkage performance of alkali-activated slag mortars. *Cem. Concr. Compos.* 76, 13–24. doi:10.1016/j.cemconcomp.2016.11.010

Ye, H., Fu, C., and Lei, A. (2020). Mitigating shrinkage of alkali-activated slag by polypropylene glycol with different molecular weights. *Constr. Build. Mater.* 245, 118478. doi:10.1016/j.conbuildmat.2020.118478

Yin, K., Jiang, Y., He, H., Ren, J., and Li, Z.(2022), Characterization of one-part alkali-activated slag with rice straw ash, *Constr. Build. Mater.* 345, 128403. doi:10.1016/j.conbuildmat.2022.128403

Yun Yang, B., and Montgomery, R. (1996). Alkaline degradation of glucose: Effect of initial concentration of reactants. *Carbohydr. Res.* 280, 27–45. doi:10.1016/0008-6215(95)00294-4

Zareei, S. A., Ameri, F., Dorostkar, F., and Ahmadi, M. (2017). Rice husk ash as a partial replacement of cement in high strength concrete containing micro silica: Evaluating durability and mechanical properties. *Case Stud. Constr. Mater.* 7, 73–81. doi:10.1016/j.cscm.2017.05.001

Zhong, P., Hu, Z., Griffa, M., Wyrzykowski, M., Liu, J., and Lura, P. (2021). Mechanisms of internal curing water release from retentive and non-retentive superabsorbent polymers in cement paste. *Cem. Concr. Res.* 147, 106494. doi:10.1016/j.cemconres.2021.106494

Zhou, C., Ren, F., Zeng, Q., Xiao, L., and Wang, W. (2018). Pore-size resolved water vapor adsorption kinetics of white cement mortars as viewed from proton NMR relaxation. *Cem. Concr. Res.* 105, 31–43. doi:10.1016/j.cemconres.2017.12.002